Results in Surfaces and Interfaces 18 (2025) 100357

Contents lists available at ScienceDirect

Results in Surfaces and Interfaces

journal homepage: www.elsevier.com/locate/rsurfi

Process parameter optimization of laser beam machining for AISI -P20 mold steel using ANFIS method

Abdullah Eaysin [a,*], Sarower Kabir [a,b], Ebru Gunister [c], Nur Jahan [a], Amir Hamza [a], Muhammad Ali Zinnah [d], Adib Bin Rashid [e]

[a] Department of Mechanical and Production Engineering, Ahsanullah University of Science and Technology, Dhaka, 1208, Bangladesh
[b] Department of Industrial, Manufacturing, & Systems Engineering, Texas Tech University, Lubbock, TX, United States
[c] Vice Dean of the Faculty of Engineering and Natural Sciences, Istanbul Health and Technology University, 34275, Istanbul, Turkey
[d] Bangladesh Council of Scientific and Industrial Research (BCSIR), Dhaka, 1205, Bangladesh
[e] Department of Mechanical Engineering, Military Institute of Science and Technology, Dhaka, 1216, Bangladesh

ARTICLE INFO

Keywords:
AISI P20
Laser beam machine (LBM)
Surface roughness
Kerf width
Adaptive neuro-fuzzy interface system (ANFIS)
Brute force

ABSTRACT

AISI P20 mold steel is commonly used for injection molds to produce plastic materials, car accessories, and electronic equipment molds. This study employed a fiber laser beam for precise machining of AISI P20 mold steel. The experimental design, based on the Taguchi 27 model, was carried out using Minitab software to optimize machining parameters, including cutting speed, gas pressure, and laser power. Surface roughness (Ra) and kerf width were the response parameters investigated. The ANFIS model, developed and analyzed using MATLAB, successfully predicted response parameters and was experimentally validated, showing improved predictions over actual measurements. The Brute Force algorithm identified the minimum combination for an optimal parameter set. The Taguchi method determined the best process parameters, indicating that cutting speed had the most significant impact. The optimum Ra was achieved with 1 m/min cutting speed, 2 bar gas pressure, and 1.8 kW laser power, while the lowest kerf width was obtained with 2 bar gas pressure, 1 m/min cutting speed, and 1.9 kW laser power. Based on the Brute Force algorithm, the minimum combination resulted in a kerf width of 0.84 mm and a surface roughness of 4.48175 μm. Microstructural analysis was performed on samples with high and low surface roughness to assess the machining surface quality.

1. Introduction

Laser beam machining (LBM) is known for its high-speed machining, precision, non-contact operation, and prolonged tool life due to minimal vibration and tool wear. This makes LBM more advantageous than conventional machining methods due to its higher accuracy and lower machining costs (Girdu and Gheorghe, 2022). LBM is particularly effective for cutting complex technical materials, delicate substances, conductive and non-conductive materials, as well as lightweight and thin components (Chen et al., 2011). Additional advantages include minimal material loss due to a narrow kerf width (Nguyen et al., 2021), smooth cutting edges with minimal mechanical deformation, and seamless integration with CNC systems for the precise machining of complex profiles (Rao et al., 2005).

AISI P20 mold steel is widely chosen for injection mold production due to its excellent hardness, strength, and wear resistance at various temperatures (Kamonpong and Janmanee, 2014). However, it is difficult to machine using conventional techniques (Amorim and Weingaertner, 2005). The use of LBM facilitates the machining of AISI P20, making it more efficient than other non-conventional methods.

Several studies have explored LBM for various materials. For instance, Rajamani and Siva Kumar investigated LBM parameters for Hastelloy C276 alloy, achieving a material removal rate (MRR) of 236.98 mg/min and a kerf taper angle of 1.135° under specific cutting conditions (Rajamani et al., 2021). Deva Nathan analyzed LBM for mild steel, identifying laser power and cutting speed as critical factors for achieving suitable surface quality and higher MRR (Devanathan et al., 2023). Kasbe's research on SS-304 revealed that increased laser power led to higher taper and surface roughness.

The Adaptive Neuro-Fuzzy Inference System (ANFIS) has been used

* Corresponding author.
E-mail addresses: abdullaheaysin6@gmail.com (A. Eaysin), sarower.mpe@aust.edu (S. Kabir), ebru.gunister@istun.edu.tr (E. Gunister), kunjojahan077@gmail.com (N. Jahan), amirhamza4823@gmail.com (A. Hamza), zinnah16bcsir@gmail.com (M.A. Zinnah), adib@me.mist.ac.bd (A.B. Rashid).

https://doi.org/10.1016/j.rsurfi.2024.100357
Received 30 August 2024; Received in revised form 3 November 2024; Accepted 17 November 2024
Available online 22 November 2024

Table 1
EDX analysis of the chemical composition of AISI P20 mold steel.

Element	Fe	Cr	Mn	Mo	C	Si	P	Cu	Co	S
wt. (%)	95.48	1.858	1.332	0.157	0.339	0.390	0.010	0.036	0.010	0.001

to predict machining outcomes due to its combination of fuzzy logic's expert knowledge and the computational power of artificial neural networks (Rajamani et al., 2021) (Mensah et al., 2020). Sengur and Ubeyli (Sengur, 2008a), (Sengur, 2008b) claim that the approach renders ANFIS modellinmore structured and relies less on experts' expertise. The system of inference built using five layers in total. Each ANFIS layer comprises numerous nodes, and the node's method is responsible for this. The previous levels' nodes function as the present layers' inputs (Çaydaş et al., 2009). The performance of the ANN model was evaluated the Erkan and F kara (Erkan et al., 2013)by comparing its predictions with previously untrained experimental results. Of the five learning algorithms tested, the LM algorithm yielded the best and fastest predictions for the damage factor and also F kara (Kara et al., 2020) investigated that in the artificial neural network modeling, the standard back-propagation algorithm was the optimal training method.Maher et al. (2014) investigated the deviation in percentage between the predicted and measured R_a for CNC milling grain standard for machining brass (60/40) and 6.25% of the end milling. This minimal inaccuracy suggests that the expected surface roughness outcome of the ANFIS model are remarkably precise compared to the actual experimental observations.

The Taguchi method is widely utilized for process optimization in engineering due to its ability to minimize experimental time while identifying optimal process parameters (Taguchi, 1987). F kara (Kara, F., n.d.) investigated that the most effective cutting parameters for Ra and Ctemp were determined through Taguchi optimization. It is extremely helpful for analysing the influence of numerous factors on performance. Taguchi-based grey correlation analysis on 17-4 PH stainless steel to identify the optimal process parameter combination for multiple output metrics (Fc, Ra, T, and Vb). The optimal settings are cutting nose radius of 0.8 mm, cutting speed of 70 m/min, and feed rate of 0.06 mm/tooth (Kara et al., 2023).The brute force algorithm offers a more direct approach than metaheuristics, and importantly, it guarantees the discovery of optimal solutions and provides evidence of their optimality (Hansen et al., 2004). Dynamic programming (a brute force method) typically involves splitting the problem into smaller sub-problems, solving each one, and retaining the solutions for later use (Kolog, 2015).

The literature review indicates that laser beam machining on various materials has been conducted using the ANFIS method to determine the percentage error disparity between the expected and actual values. However, there is a shortage of research utilizing ANFIS models to predict the behavior of AISI P20 mold steel, as well as a lack of optimization techniques to identify the suitable combination of input parameters for laser beam machining. Moreover, the Brute Force algorithm has not been widely implemented to identify optimal combinations of LBM input parameters. This research addresses these gaps by predicting the cutting parameters for the LBM process using the ANFIS model and utilizing the Taguchi L_{27} model to improve machining parameters. The combination of surface roughness (R_a) and kerf width will be integrated to find the best operating conditions, ensuring high-quality output using the Brute Force algorithom and conduct a microstructural analysis on samples exhibiting both high and low surface roughness in order to evaluate the quality of the machined surfaces.

2. Material and methods

2.1. Materials

P20 tool steel is known as a low-C plastic Mold steel, composed of chromium as an alloying component. Table 1 shows the chemical composition of the AISI P20 mold steel utilized in this work as determined by EDX.

Table 2
The AISI P20 mold steel has different conditions and mechanical characteristics (On).

Properties		Conditions T (°C)
Density (kg/m^3)	7.86x10^3	30
Ratio of Poisson's	0.26–0.30	30
Modulus of Elasticity (GPa)	180–210	30
Thermal Expansion coefficient (1/°C)	13.8x10^{-6}	30–425

Table 3
Taguchi L_{27} model.

Cutting parameter	Factor	Unit	Level		
			1	2	3
Laser Power (LP)	A	KW	1.8	1.9	2
Gas Pressure (GP)	B	Bar	1.3	1.7	2
Cutting Speed (V)	C	m/min	0.5	0.8	1

AISI P20 mold steel is renowned for its exceptional resistance to softening at elevated temperatures (Farhat, 2003). It is specifically utilized in applications such as zinc casting through die and molding processes for plastic. Common uses include plastic molds, hydroforming tools, and frames for plastic pressure dies. Freezing metals has been recognized for many years as an effective method for enhancing the wear life and hardness of tool steel (Al Javed and Bin Rashid, 2024). Subzero temperatures significantly influence the mechanical characteristics, hardness, and microstructure of tool steel. This direct improvement in the service life of tool steel in industrial applications is noteworthy (Priyadarshini et al., 2020). The AISI P20 mold steel exhibits varying conditions and mechanical properties, as shown in Table 2.

2.2. Experimental plan

The experimental process from material selection to optimization of the response parameters is given in Fig. 1.

A Bodor laser model F3015, as shown in Fig. 2(a), was used in this study to cut square-shaped AISI P20 material measuring 1.5 × 1.5 cm in 27 individual runs, as illustrated in Fig. 3(b). Input parameters considered included cutting speed, laser power, and gas pressure. Each parameter varied across three levels, as detailed in Table 4. The data set for the input parameters was generated using the Taguhi L_{27} method. In the Taguchi combination model, each input parameter was used three times to account for errors from the experiments. The parameter set was based on pilot runs of the AISI P20 material, with three pilot runs conducted for varied input/process parameter data. In this experiment, 27 samples were created using factor and level data to determine the response parameters Ra and kerf width. The ANFIS technique used for the training data set is based on the educational and testing data provided in Table 5. The Taguchi L_{27} orthogonal array employed a smaller-the-better signal-to-noise ratio to identify the optimal points for the response parameters. The brute force algorithm identified the data set with the minimum response parameters, as selecting the minimum values for Ra and kerf width indicates better machinability. Roughness, heat-affected zone, and kerf width were measured.

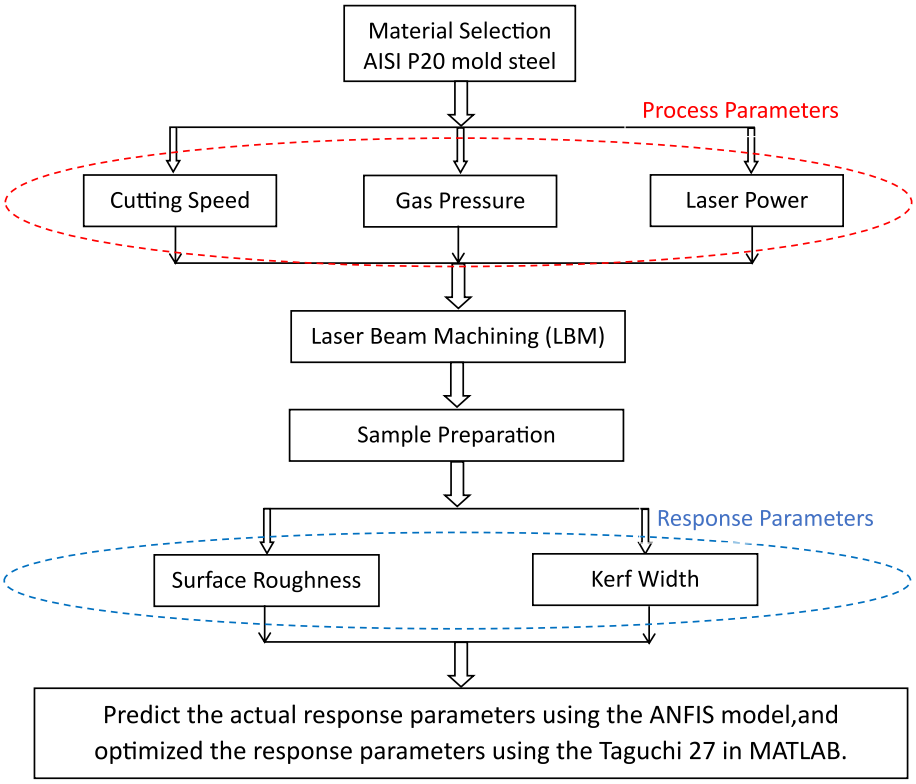

Fig. 1. Schematic diagram of the whole experimental procedure.

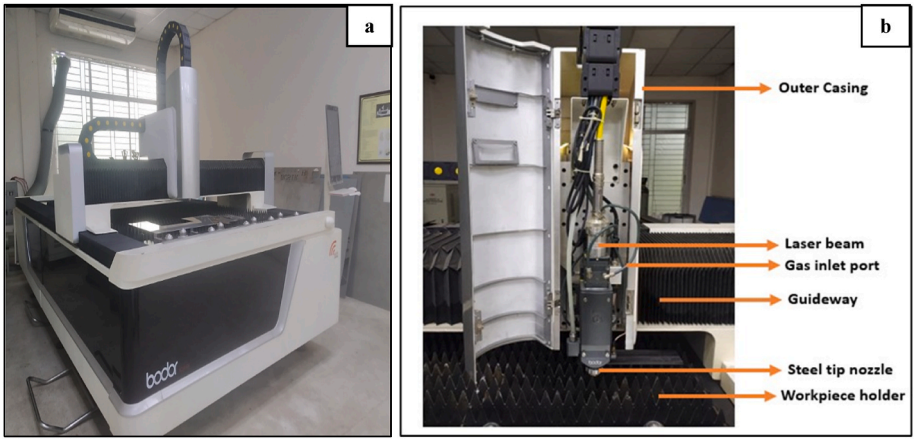

Fig. 2. (a) Laser cutting machine, and (b) Head of the LBM.

2.2.1. Surface roughness measurements

Surface roughness is commonly used as a quality measure and is often a technical requirement for mechanical objects. Achieving a proper surface quality is crucial for the functional behaviour of a component. The most frequent technique requires selecting conservative process parameters, which neither assure the smoothness of the surface needed nor achieve high metal removal rates (Benardos and Vosniakos, 2003). The surface tester equipment will determine the surface roughness. Mitutoyo brand (SJ-210 series) is shown in Fig. 4. The samples are securely held in place using a vice during the measurement process. To obtain measurements, the side of the sample is carefully swiped. Surface roughness measurements are taken on each side of the machining site. Afterward, the average value of the four sides is calculated to determine the actual surface roughness value, R_a. This approach ensures that for one sample, four times readings are taken from different sides of the sample, which helps to capture variations in surface roughness. A more representative and reliable value for Ra can be obtained by averaging the measurements.

Surface roughness is commonly used as a quality measure and is often a technical requirement for mechanical components. Achieving proper surface quality is crucial for the functional behavior of a component. The most common technique involves selecting conservative process parameters, which do not ensure the smoothness of the surface required nor achieve high metal removal rates (Benardos and Vosniakos, 2003). Surface roughness will be determined using a Mitutoyo brand surface tester (SJ-210 series), as shown in Fig. 4. The samples are securely held in place using a vice during the measurement process. To obtain measurements, the side of the sample is carefully swiped. Surface roughness measurements are taken on each side of the machining site. Afterward, the average value of the four sides is

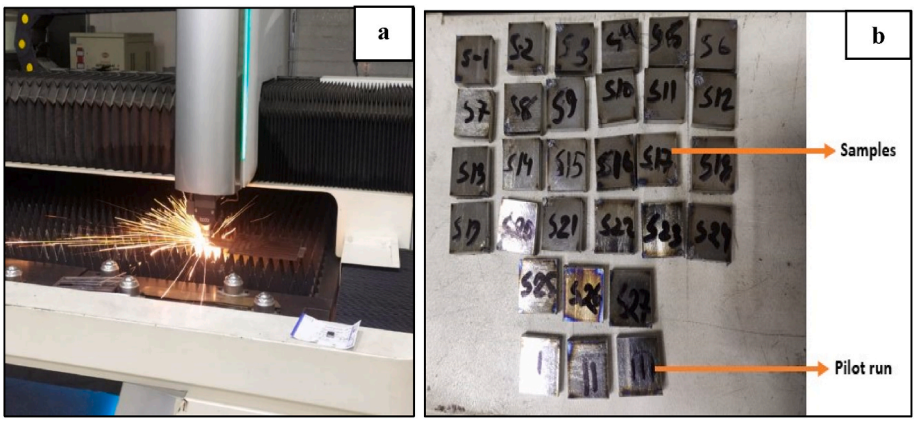

Fig. 3. (a) Machining of the P20 sheet and (b) P20 samples after machining.

Table 4
Investigation result for the Taguchi L_{27} model.

Sample no	LP(KW)	GP(Bar)	V(m/min)	d (mm)	R_a (μm)
1	1.8	1.3	0.5	0.77	6.472
2	1.8	1.3	0.5	0.80	5.886
3	1.8	1.3	0.5	0.77	6.866
4	1.8	1.7	0.8	0.92	5.486
5	1.8	1.7	0.8	0.72	5.397
6	1.8	1.7	0.8	0.83	5.325
7	1.8	2	1	0.60	4.767
8	1.8	2	1	0.61	5.468
9	1.8	2	1	0.66	4.737
10	1.9	1.3	0.8	0.82	5.664
11	1.9	1.3	0.8	0.81	6.070
12	1.9	1.3	0.8	0.80	5.613
13	1.9	1.7	1	0.65	5.387
14	1.9	1.7	1	0.54	6.263
15	1.9	1.7	1	0.66	6.567
16	1.9	2	0.5	0.58	6.649
17	1.9	2	0.5	0.84	6.938
18	1.9	2	0.5	0.83	5.590
19	2	1.3	1	0.64	6.763
20	2	1.3	1	0.84	4.482
21	2	1.3	1	0.60	6.003
22	2	1.7	0.5	0.81	6.708
23	2	1.7	0.5	0.83	10.634
24	2	1.7	0.5	0.80	7.479
25	2	2	0.8	0.83	6.343
26	2	2	0.8	0.69	5.589
27	2	2	0.8	0.68	5.488

calculated to determine the actual surface roughness value, R_a. The standards for test samples and deniers for surface roughness measurement ensure samples are cleaned and free of oil, grease, or debris. Use ISO 4287 and ISO 4288 for roughness parameters like Ra and Rz. Utilize stylus profilometers for contact-based measurements, capturing Ra. Maintain a minimum sample area of 10 mm × 10 mm for accurate readings and take measurements at multiple points for uniform data. Note that "deniers" are not related to surface roughness measurements.

2.2.2. Kerf width measurements

The process of measuring the kerf is straightforward. Begin by creating a section with a known measurement, such as a 1.5 cm square, and carefully measure its actual width. To measure the kerf width, use digital slide callipers. In Fig. 5, assume the initial width is x_1, and the final width is x_2. Therefore, the kerf width (d) can be calculated as x_1 - x_2. When measuring the actual (final) width of the P20 sample, use the internal jaw of the slide calliper equipment. When measuring the initial width, use the external jaw of the slide callipers equipment.

2.2.3. Prediction process using the ANFIS method

A neuro-fuzzy inference adaptive system is a combination of prediction models; it combines neural networks and fuzzy logic skills to establish a mapping relationship. The response parameters considered for analysis were gas pressure, cutting speed, and laser power. The ANFIS model employed logical OR operations among multiple layers. In Fig. 6, the resultant information of the initial layer was used to generate subsequent layers. Initially, three membership values were assigned to the cutting speed, gas pressure and laser power inputs to create the first layer. The initial layer's result becomes the input used for the following layer, where the firing strength was calculated using OR logic operations. And determine the third layer. In third layer, the values were normalized. In the fourth layer, the value was obtained through defuzzification of the consequent part of the rules by summing the output of all third-layer nodes, resulting in the response parameters. Finally, Aggregate the defuzzification consistently and obtaining the output values.

This work performed the ANFIS using the antisemite function in MATLAB R2023a. That create the interface for training and testing data and is needed to give the fuzzy rule for finding the response parameter predicted value for each actual response parameter. The model developed was verified based on the ANFIS model's existing experiment.

$$R^2 = 1 - \left(\frac{\sum_j \left(O_{prei} - O_{expi} \right)^2}{\sum_j \left(O_{prei} \right)^2} \right) \tag{1}$$

In Equation (1), O_{prei} and O_{expi} represent the predicted and experimental output, while i to j represent the number of paired input/outputs.

2.2.4. The Taguchi L27 approach is used in the optimization process

Taguchi analysis is used to optimize the parameters. Three methods of analysis are utilized: nominal-the-best, larger-the-best, and smaller-the-best. In this study, the smaller-the-best technique is recommended to assess the influence levels of experimental parameters in determining the surface roughness (R_a) optimal values and kerf width. The smaller-the-better strategy is represented by Equation (2).

$$\eta = -10 \log_{10} \left(\frac{1}{n} \sum_{i=1}^{n} Y_{ij}^2 \right) \tag{2}$$

In Equation (2), η represents the sound-to-noise ratio, n represents the total number of states in the variable-level combinations, and Y represents the response for the specified combination of component levels. In the case of each characteristic, the S/N ratio transformation is applied. It is important to note that a greater S/N ratio suggests a superior outcome.

In Taguchi method, various models for experimental design are commonly utilized (26, 27). The L_{27} model (33) was chosen for this study's smaller-is-better approach. Taguchi L_{27} model (3^3) consists of

Table 5
Experimental prediction value of response parameters.

sample	LP	GP	V	$R_{aActual}$		$R_{aPredicted}$	$Error_{Ra}$ (%)	d_{Actual}		$d_{Predicted}$	$Error_{d}$ (%)
1	1.8	1.3	0.5	6.47	**Training data**	6.41	0.99	0.77	**Training data**	0.78	−1.3
2	1.8	1.3	0.5	5.89		6.41	−8.86	0.80		0.78	2.5
3	1.8	1.3	0.5	6.87		6.41	6.67	0.77		0.78	−1.3
4	1.8	1.7	0.8	5.49		5.40	1.52	0.92		0.82	10.5
5	1.8	1.7	0.8	5.40		5.40	−0.10	0.72		0.82	−14.4
6	1.8	1.7	0.8	5.32		5.40	−1.46	0.83		0.82	0.8
7	1.8	2	1	4.77		4.99	−4.69	0.60		0.62	−3.9
8	1.8	2	1	5.47		4.99	8.73	0.61		0.62	−2.2
9	1.8	2	1	4.74		4.99	−5.36	0.66		0.62	5.6
10	1.9	1.3	0.8	5.66		5.78	−2.09	0.82		0.81	1.2
11	1.9	1.3	0.8	6.07		5.78	4.74	0.81		0.81	0.0
12	1.9	1.3	0.8	5.61		5.78	−3.02	0.80		0.81	−1.2
13	1.9	1.7	1	5.39		6.07	−12.72	0.65		0.62	5.1
14	1.9	1.7	1	6.26		6.07	3.05	0.54		0.62	−14.2
15	1.9	1.7	1	6.57		6.07	7.53	0.66		0.62	6.6
16	1.9	2	0.5	6.65		6.39	3.86	0.58		0.75	−29.3
17	1.9	2	0.5	6.94		6.39	7.86	0.84		0.75	10.7
18	1.9	2	0.5	5.59		6.39	−14.35	0.83		0.75	9.6
19	2	1.3	1	6.76		5.75	14.99	0.64		0.69	−8.3
20	2	1.3	1	4.48		5.75	−28.28	0.84		0.69	17.5
21	2	1.3	1	6.00		5.75	4.22	0.60		0.69	−15.6
22	2	1.7	0.5	6.71		6.81	−1.55	0.81		0.81	0.0
23	2	1.7	0.5	6.25		6.81	−8.93	0.83		0.81	2.0
24	2	1.7	0.5	7.48		6.81	8.91	0.80		0.81	−1.7
25	2	2	0.8	6.34		6.34	0.00	0.83		0.83	0.0
26	2	2	0.8	5.59	**Testing data**	6.34	−13.49	0.69	**Testing data**	0.83	−20.3
27	2	2	0.8	5.49		6.34	−15.57	0.68		0.83	−22.1

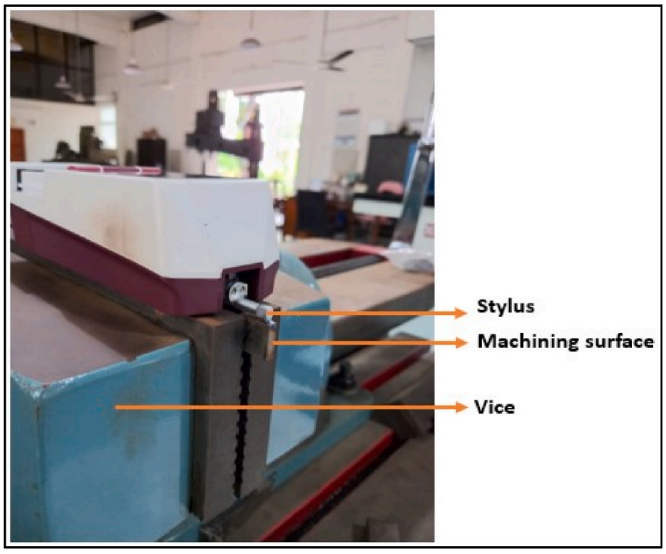

Fig. 4. Measuring surface roughness.

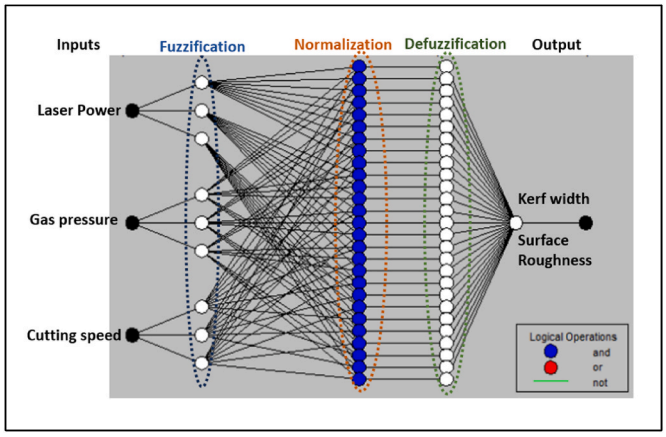

Fig. 6. Structure of an adaptive neuro-fuzzy interface system for Ra and kerf width.

three factors, namely the speed of cutting (CS), laser power (LP), and gas pressure (GP), each with three levels (as listed in Table 3).

Implementing the Taguchi L_{27} model requires conducting 27 experiments. Two experimental results were obtained From each test, namely Surface Roughness (R_a) and kerf width (d). All The investigation

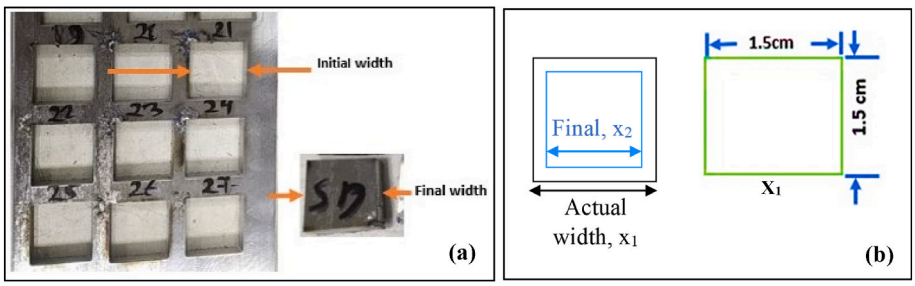

Fig. 5. (a) kerf width measurement, and (b) for one square sheet dimensions.

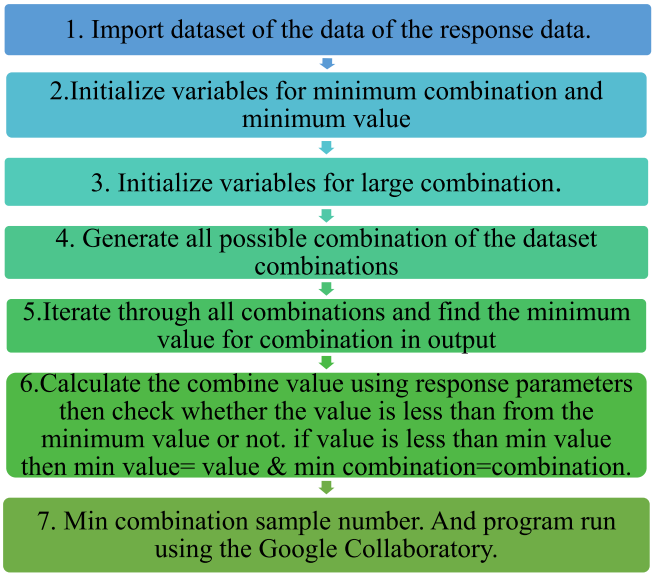

Fig. 7. Process of the Brute force method.

outcomes are depicted in Table 4.

2.2.5. Multi-optimization process using the brute force method

Brute force methods try to calculate all possible solutions and decide which is the best. For the study of this experiment, the Brute force method was used to calculate the optimum minimum data set of the response parameters. There were several steps for applying the brute force covered in Fig. 7.

2.2.6. Microscopic view of machining surface

The NMM-800TRF light microscope was utilized to accurately observe and analyse the presence of internal cracks, defects, and surface roughness on the machined surface. To achieve this, the sample cutting surfaces were carefully positioned under the objective lenses, with both the coarse and fine adjustments made to ensure a clear microscopic view. The choice of objective lens, either 100x or 200x, was determined based on the clarity of the microscopic view obtained. By employing these different objective lenses, we could closely examine the machining surface from multiple perspectives, allowing for a comprehensive evaluation of the smallest details and features present. Specifically, the focus was placed on per sample four machining side to examining sample, as it provided valuable insights into the tiniest components and characteristics of interest.

3. Result and discussion

3.1. ANFIS (Adaptive neural fuzzy interface system) prediction

The prediction value was determined using an ANFIS. The neural network was trained using 27 experimental trials, each class they represented. Table 4 contains the specifics. The neural network structure consisted of five layers: four for input and one for output. The structure membership function (Mfs) Triangular Membership Function number of mfs 3-3-3 was chosen based on the overall model accuracy. The classification model was designed using the MATLAB neural pattern recognition tool. The structure of ANFIS is shown in Fig. 6. The training and testing ratios were 90% and 10%, respectively. As a result, there were 25 data points accessible for training the system and 2 data points accessible for testing. The iteration number was 100 epochs for the training data and testing data. The general FIS was selected as a grid partition to split the problem into smaller problems. The Mean Squared Error (MSE) value for the given actual and predicted R_a and kerf width values is approximately 20% and 0.55%.The model has shown an average testing error of 6.29% for the surface roughness (Fig. 8). The obtained predicted value of the R_a and kerf width values is given in Table 5.

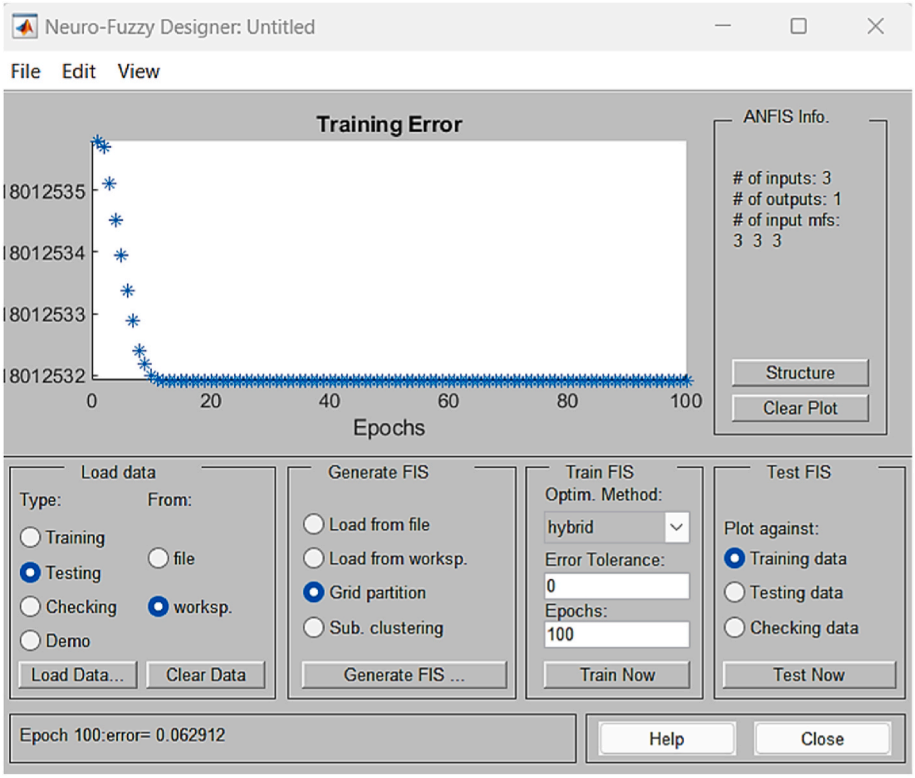

Fig. 8. Training data processing.

$$\text{Prediction error percentage} = \left(\frac{(\text{experimental value} - \text{prediction value})}{\text{experimental value}}\right)*100$$

This prediction error indicates the percentage of deviation from the actual value.

The study of Fig. 9 reveals that the accuracy of the surface roughness (R_a) data for both response parameters is shown. For the surface roughness (R_a) parameter, the anticipated ($R_{aPredicted}$) and actual ($R_{aActual}$) values have a positive linear correlation. This indicates that as $R_{aPredicted}$ increases, $R_{aActual}$ also tends to increase. The surface roughness data's accuracy is represented by an R^2 value of 0.4766, representing 47.66% accuracy, indicating a medium positive correlation. The Adjusted R^2 value of the surface roughness 0.4448 means 44.48%. The value of the adjusted R^2 represents the more precise value that fits with the baseline.

For the kerf width parameter, the accuracy of the kerf width shows R^2 value of 0.4679, which means 46.79% accuracy, representing a medium correlation. The Adjusted R^2 value of the kerf width 0.4458 means 44.58%. The value of the adjusted R^2 represents the more precise value that fits with the baseline.

In illustrated Figs. 10 and 11, the measured actual values of surface roughness and kerf width are depicted, showing variations and fluctuations. No clear trend was observed in the data. Instead, significant deviations are observed at multiple points, particularly in the surface roughness measurements rather than the kerf width. The surface's roughness variations can be attributed to inherent random errors within the manufacturing process or system. Initially, the R_a values align well with the predicted values, indicating good accuracy. However, as more samples are taken, the surface roughness standard deviation increases and the measurements deviate from the mean. In the comparison graphs for kerf width, it can be observed that around 50% of the values align closely with the predicted values. These variations involving surface roughness can be attributable to defects in manufacturing. The maximum deviation in surface roughness is found for sample 20, with an error of −28.8%. For the kerf width, the maximum deviation occurs in sample 16, with an error of −29.3%. It is important to note that these fluctuations and deviations highlight random errors and variations within the manufacturing process.

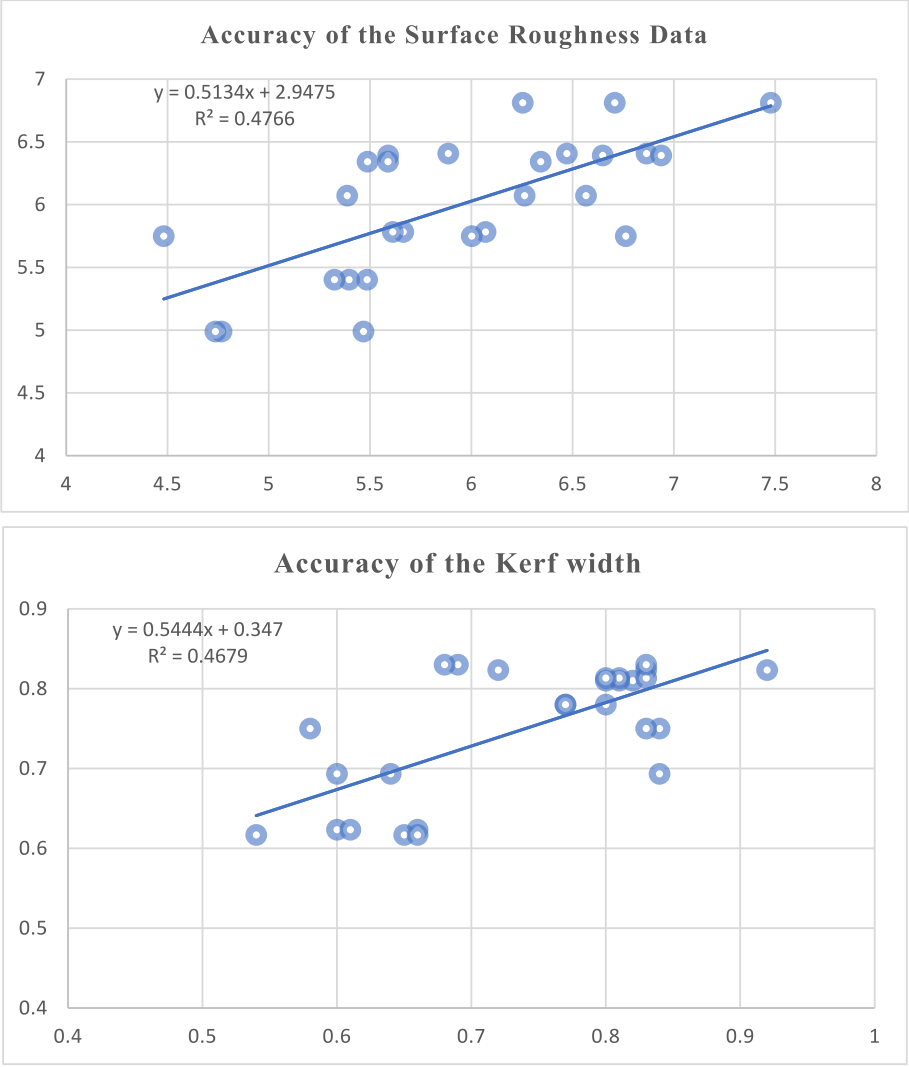

Fig. 9. Coefficient of determination (R^2) for both response parameters data.

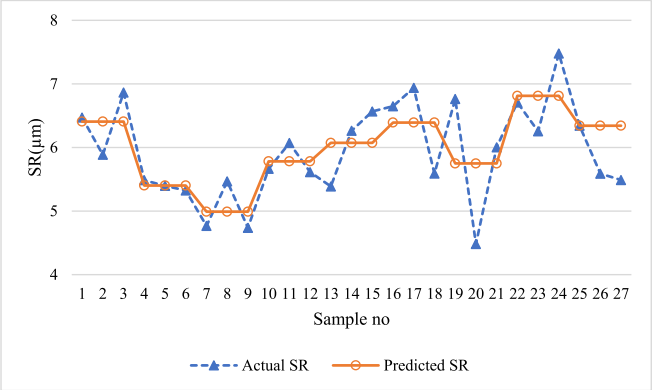

Fig. 10. Actual and predicted surface roughness's are compared.

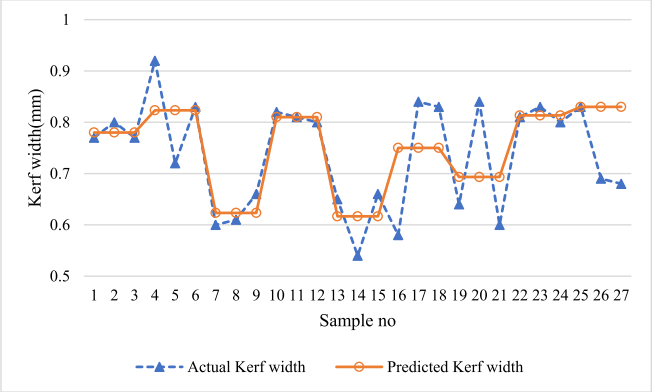

Fig. 11. Actual and predicted kerf width are compared.

3.2. Taguchi L_{27} orthogonal array optimization

In Fig. 12, it can be observed that the different machining process parameters, such as gas pressure, gas pressure, and laser power, influence the ratio of Signal-to-Noise (S/N). The ratio of S/N was chosen to be smaller, which is better since a lower number suggests smoother surface roughness, which is desired. Therefore, at the higher S/N point, the minimum surface roughness is found.

Table 6 illustrates the ranking of process parameters in order of their impact on surface roughness. Cutting speed holds the highest rank, followed by laser power and gas pressure. This implies that cutting speed has the greatest influence on surface roughness next to gas pressure, as well as laser power. Based on the analysis, gas pressure at level 1, cutting speed at level 3, and laser power at level 1 are the optimal points for surface roughness. It indicates that the optimum process parameters for achieving the lowest surface roughness are 2 bar of gas pressure, 1 m/min cutting speed, and 1.8 KW of laser power.

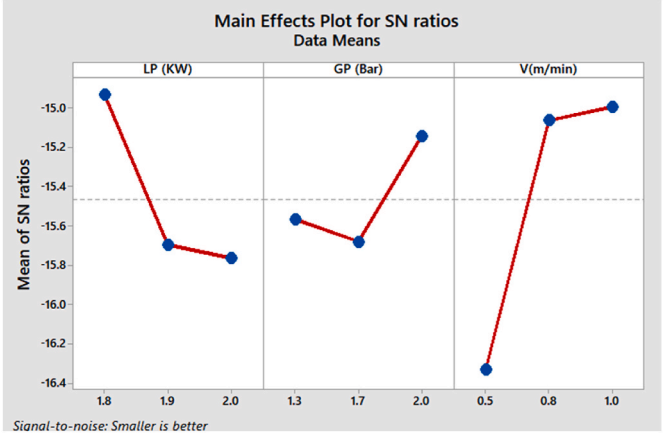

Fig. 12. S/N ratio for the R_a.

Table 6
Smaller-is-better.

Level	LP (KW)	GP (Bar)	V(m/min)
1	−14.93	−15.57	−16.94
2	−15.70	−16.29	−15.07
3	−16.38	−15.14	−15.00
Delta	1.45	1.15	1.95
Rank	2	3	1

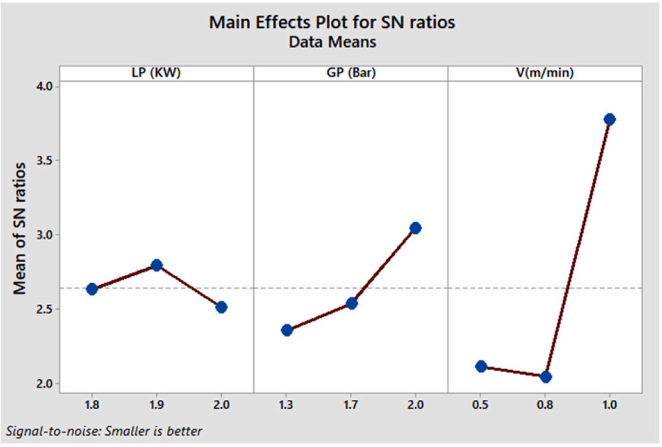

Fig. 13. S/N ratio for the kerf width.

Table 7
Smaller is better.

Level	LP (KW)	GP (Bar)	V(m/min)
1	2.633	2.356	2.113
2	2.795	2.535	2.044
3	2.511	3.048	3.782
Delta	0.284	0.691	1.738
Rank	3	2	1

Fig. 13 shows kerf width always minimum that indicates lower material vaporized with the machining with laser. So, at the higher S/N ratio point found the minimum kerf width.

The highest rank of process parameter that impacts the kerf width is cutting speed, which corresponds to the next rank, gas pressure, and the last laser power (Table 7). So, for the kerf width, the optimum point, the minimum kerf width, is found in gas pressure level 2, cutting speed level 2, and laser power level 3. The lowest kerf width can be achieved at optimum process parameters such as gas pressure 2 bar, cutting speed 1 m/min, and laser power 1.9 KW.

3.3. Multi-optimization brute force method

The Brute Force algorithm finds the finest dataset with minimum value. Used Python to do this code.

```
import itertools
dataset = [
[0.77, 6.4715], [0.8, 5.886], [0.77, 6.8655], [0.92, 5.4855], [0.72, 5.397], [0.83, 5.3245], [0.6, 4.7665], [0.61, 5.4675],[0.66, 4.7365], [0.82, 5.66425] [0.81, 6.07025], [0.8, 5.61275], [0.65, 5.38725], [0.54, 6.263],[0.66, 6.5665], [0.58, 6.6485], [0.84, 6.9375], [0.83, 5.58975], [0.64, 6.763], [0.84, 4.48175], [0.6, 6.0025], [0.81, 6.70825], [0.83, 10.634], [0.8,7.47875], [0.83, 6.34275], [0.69, 5.589], [0.68, 5.488]
```

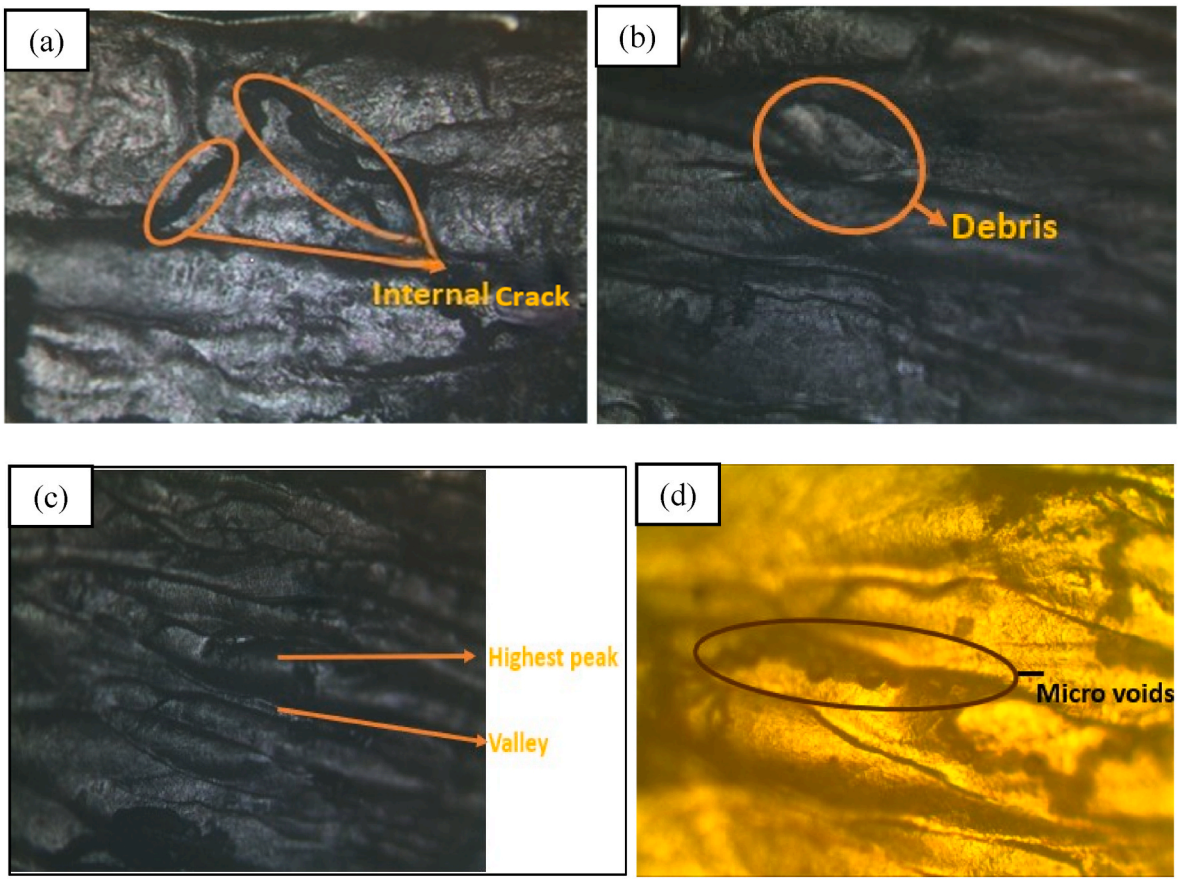

Fig. 14. (a) Microscopic view 200X of sample 20, (b–d) Microscopic view 100X of sample 24.

```
]
#Initialize variables for minimum combination and minimum value
min_combination = None
min_value = float('inf') # Initialize with a large value.
# Generate all possible combinations of the dataset
combinations = list(itertools.combinations(dataset, 1))
# Iterate through all combinations and find the minimum value
for combination in combinations:
output1, output2 = zip(*combination)
value = sum(output1) + sum(output2)
# Calculate the combined value
if value < min_value:
min_value = value
min_combination = combination
sample = dataset. Index(min_combination[0])
print (sample + 1)
# Print the minimum value and combination.
# print ("Minimum value:", min_value)
print ("Minimum combination:", min_combination[0]).
```

Result of the Brute force method is sample 20 minimum combination: [0.84,4.48175]. It shows that the minimum combination kerf width 0.84 mm and surface roughness 4.48175 μm.

3.4. Microscopic view observation

In Fig. 14 (a), it is evident that there is an internal crack apparent in the microscopic view. This microscopic view corresponds to the sample with the smallest surface roughness value. Contrastingly, in Fig. 14 (b), unwanted material is present on the surface, which seems to have impinged into the surface. This is observed in the sample with the highest surface roughness value. Furthermore, in Fig. 14 (c), a clear visualization of the peaks and valleys can be seen. This results from the higher surface roughness of the sample being depicted. Fig. 14 (d) shows the microvoid defects at 100X microscopic view. After observations, the differences in surface characteristics are highlighted based on the surface roughness values. The presence of internal cracks, unwanted material, micro void and the visibility of peaks and valleys can provide insights into the surface quality and roughness of the examined material.

4. Conclusion

This work aimed to machine AISI P20 mold steel using a laser cutting machine, involving parameter optimization and prediction. Taguchi L_{27} orthogonal array was used as the purpose of the experimental design. Process machining parameter interaction of gas pressure, cutting speed and laser power. Membership functions were established using a 3-3-3 ANFIS structure neural network. These models were then utilized to find optimal predicted solutions. The key conclusions can be outlined as follows:

- The Signal-to-Noise (S/N) ratio was used for single optimization, indicating that higher S/N ratio levels correspond to minimum response parameters, including surface roughness and kerf width.
- Specific combinations of 2 bar gas pressure, 1 m/min cutting speed, and 1.8 kW laser power achieved a smooth surface.
- The optimal minimal material vaporization during laser cutting was achieved with a combination of 2 bar gas pressure, 1 m/min cutting speed, and 1.9 kW laser power.
- The brute force algorithm was employed as a multi-optimization technique to identify the best minimal dataset for the response parameters.

- Results indicated that sample 20 (2 kW, 1.3 bar, 1 m/min) provided the optimum minimum dataset, exhibiting the lowest surface roughness.
- Microscopic investigation of sample 20 at 200x magnification revealed smooter surface and presence of internal cracks on the surface.In contrast, higher roughness samples displayed irregularities with prominent peaks and valleys.Sample 24 (2 kW, 1.7 bar, 0.5 m/min) at 100x magnification showed the presence of microvoid debris on the machining surface.

In future studies, examining the potential thermal effects of the light from the laser striking the substance is critical. The heat-affected zone (HAZ) and annealing of the material's microstructure width should be investigated. Different neural network models can also be compared to determine which provides the most accurate data based on real-world observations. Alternative optimization algorithms like genetic algorithms can be explored to achieve the maximum dataset level. These aspects will be addressed in future experimental processes.

CRediT authorship contribution statement

Abdullah Eaysin: Writing – original draft, Methodology, Investigation, Formal analysis, Conceptualization. **Sarower Kabir:** Writing – review & editing, Supervision, Project administration, Conceptualization. **Ebru Gunister:** Writing – review & editing, Visualization, Validation, Supervision. **Nur Jahan:** Writing – original draft, Methodology, Investigation, Conceptualization. **Amir Hamza:** Writing – original draft, Methodology, Investigation, Formal analysis, Conceptualization. **Muhammad Ali Zinnah:** Visualization, Software, Resources, Investigation. **Adib Bin Rashid:** Writing – review & editing.

Declaration of competing interest

The authors declare that they have no known competing financial interests or personal relationships that could have appeared to influence the work reported in this paper.

Data availability

Data will be made available on request.

References

Al Javed, M.O., Bin Rashid, A., 2024. Laser-assisted micromachining techniques: an overview of principles, processes, and applications. Adv. Mater. Process. Technol. 1–44. https://doi.org/10.1080/2374068X.2024.2397156.

Amorim, F.L., Weingaertner, W.L., 2005. The influence of generator actuation mode and process parameters on the performance of finish EDM of a tool steel. J. Mater. Process. Technol. 166 (3), 411–416. https://doi.org/10.1016/j.jmatprotec.2004.08.026.

Benardos, P.G., Vosniakos, G.C., 2003. Predicting surface roughness in machining: a review. Int. J. Mach. Tool Manufact. 43 (8), 833–844. https://doi.org/10.1016/S0890-6955(03)00059-2.

Çaydaş, U., Hasçalik, A., Ekici, S., 2009. An adaptive neuro-fuzzy inference system (ANFIS) model for wire-EDM. Expert Syst. Appl. 36 (3 PART 2), 6135–6139. https://doi.org/10.1016/j.eswa.2008.07.019.

Chen, M.F., Sen Ho, Y., Hsiao, W.T., Wu, T.H., Tseng, S.F., Huang, K.C., 2011. Optimized laser cutting on light guide plates using grey relational analysis. Opt Laser. Eng. 49 (2), 222–228. https://doi.org/10.1016/j.optlaseng.2010.09.008.

Devanathan, C., Giri, R., Dhandapani, S., Muthiah, C.T., Sivanand, A., 2023. A study on laser beam machining and prediction of surface finish and material removal rate by fuzzy clustering. Lect. Notes Mechan. Eng. 507–518. https://doi.org/10.1007/978-981-19-3895-5_41.

Erkan, Ö., Işık, B., Çiçek, A., Kara, F., 2013. Prediction of damage factor in end milling of glass fibre reinforced plastic composites using artificial neural network. Appl. Compos. Mater. 20 (4), 517–536. https://doi.org/10.1007/s10443-012-9286-3.

Farhat, Z.N., 2003. Microstructural Characterization of WC-TiC-Co Cutting Tools during High-Speed Machining of P20 Mold Steel, vol. 51, pp. 117–130. https://doi.org/10.1016/j.matchar.2003.10.005.

Girdu, C.C., Gheorghe, C., 2022. Energy esfficiency in CO2 laser processing of hardox 400 material. Materials 15 (13). https://doi.org/10.3390/ma15134505.

Hansen, E.A., Bernstein, D.S., Zilberstein, S., 2004. Dynamic programming for partially observable stochastic games. AAAI Workshop - Techn. Rep. WS-04–08 (2000), 25–30.

Kamonpong, J., Janmanee, P., 2014. Deep Hole of AISI P20 Mold Steel Material by Electrical Discharge Machining, vol. 590, pp. 244–248. https://doi.org/10.4028/www.scientific.net/AMM.590.244.

Kara, F., Karabatak, M., Ayyildiz, M., Nas, E., 2020. Effect of machinability, microstructure and hardness of deep cryogenic treatment in hard turning of AISI D2 steel with ceramic cutting. J. Mater. Res. Technol. 9 (1), 969–983. https://doi.org/10.1016/j.jmrt.2019.11.037.

Kara, F., n.d. Experimental and statistical investigation of the effect of nanoparticle minimum quantity lubrication(nano-MQL)method on cutting performance. Gazi J. Eng. Sci. 10, 102–113.

Kara, F., Bulan, N., Akgün, M., Köklü, U., 2023. Multi-objective optimization of process parameters in milling of 17-4 PH stainless steel using taguchi-based gray relational analysis. Eng. Sci. 26, 1–12. https://doi.org/10.30919/es961.

Kolog, E.A., 2015. Dynamic Programming Using Brute Force Algorithm for a Traveling Salesman Problem. https://doi.org/10.13140/RG.2.1.2304.2727. June.

Maher, I., Eltaib, M.E.H., Sarhan, A.A.D., El-Zahry, R.M., 2014. Investigation of the effect of machining parameters on the surface quality of machined brass (60/40) in CNC end milling - ANFIS modeling. Int. J. Adv. Manuf. Technol. 74 (1–4), 531–537. https://doi.org/10.1007/s00170-014-6016-z.

Mensah, R.A., Xiao, J., Das, O., Jiang, L., Xu, Q., Alhassan, M.O., 2020. Application of adaptive neuro-fuzzy inference system in flammability parameter prediction. Polymers 12 (1), 1–16. https://doi.org/10.3390/polym12010122.

Nguyen, D.T., Ho, J.R., Tung, P.C., Lin, C.K., 2021. Prediction of kerf width in laser cutting of thin non-oriented electrical steel sheets using convolutional neural network. Mathematics 9 (18). https://doi.org/10.3390/math9182261.

D. R. On, '" MACHINING PERFORMANCE of AISI P20 STEEL with GRAPHITE and TUNGUSTEN BASED ELECTRODE on EDM ' Submitted in Partial Fulfilment of the Requirements for Award of Degree of".

Priyadarshini, M., Behera, A., Biswas, C.K., 2020. Effect of sub-zero temperatures on wear resistance of AISI P20 tool steel. J. Braz. Soc. Mech. Sci. Eng. 42 (5), 1–13. https://doi.org/10.1007/s40430-020-02298-2.

Rajamani, D., Siva Kumar, M., Balasubramanian, E., Tamilarasan, A., 2021. Nd: YAG laser cutting of Hastelloy C276: ANFIS modeling and optimization through WOA. Mater. Manuf. Process. 36 (15), 1746–1760. https://doi.org/10.1080/10426914.2021.1942910.

Rao, B.T., Kaul, R., Tiwari, P., Nath, A.K., 2005. Inert gas cutting of titanium sheet with pulsed mode CO2 laser. Opt Laser. Eng. 43 (12), 1330–1348. https://doi.org/10.1016/j.optlaseng.2004.12.009.

Sengur, A., 2008a. Wavelet transform and adaptive neuro-fuzzy inference system for color texture classification. Expert Syst. Appl. 34 (3), 2120–2128. https://doi.org/10.1016/j.eswa.2007.02.032.

Sengur, A., 2008b. An expert system based on principal component analysis, artificial immune system and fuzzy k-NN for diagnosis of valvular heart diseases. Comput. Biol. Med. 38 (3), 329–338. https://doi.org/10.1016/j.compbiomed.2007.11.004.

Taguchi, G., 1987. Taguchi on Robust Technology Development: Bringing.